NANO LETTERS

2007
Vol. 7, No. 12
3759−3765

# A Cellular Trojan Horse for Delivery of Therapeutic Nanoparticles into Tumors

**Mi-Ran Choi,[†] Katie J. Stanton-Maxey,[†] Jennifer K. Stanley,[†] Carly S. Levin,[‡,§] Rizia Bardhan,[‡,§] Demir Akin,[||] Sunil Badve,[⊥] Jennifer Sturgis,[#] J. Paul Robinson,[#] Rashid Bashir,[||,#] Naomi J. Halas,[‡,§,+] and Susan E. Clare*[,†]**

*Department of Surgery, Indiana University School of Medicine, Indianapolis, Indiana 46202, Department of Chemistry, Rice University, Houston, Texas 77005, Department of Electrical and Computer Engineering, Rice University, Houston, Texas 77005, Birck Nanotechnology Center, Purdue University, West Lafayette, Indiana 47907, Department of Pathology and Laboratory Medicine, Indiana University School of Medicine, Indianapolis, Indiana 46202, Bindley BioScience Center, Purdue University, West Lafayette, Indiana 47907, and Laboratory for Nanophotonics, Rice University, Houston, Texas 77005*

*Received August 31, 2007; Revised Manuscript Received September 25, 2007*

**ABSTRACT**

**Destruction of hypoxic regions within tumors, virtually inaccessible to cancer therapies, may well prevent malignant progression. The tumor's recruitment of monocytes into these regions may be exploited for nanoparticle-based delivery. Monocytes containing therapeutic nanoparticles could serve as "Trojan Horses" for nanoparticle transport into these tumor regions. Here we report the demonstration of several key steps toward this therapeutic strategy: phagocytosis of Au nanoshells, and photoinduced cell death of monocytes/macrophages as isolates and within tumor spheroids.**

Nanotechnology shows great promise for the diagnosis and treatment of cancer. Nanoparticle-based therapeutics have been successfully delivered into tumors by exploiting the enhanced permeability and retention (EPR) effect, a property that permits nanoscale structures to be taken up passively into tumors without the assistance of antibodies or other targeting moieties.[1] Nanoparticle-based therapies have also been targeted to malignant cells by conjugating the nanoparticles with antibodies or peptides specific to those cells.[2] An alternative strategy for delivering nanoparticle-based therapies within the tumor microenvironment, not previously explored, involves the uptake of nanoparticles within nonmalignant cells which subsequently are recruited into the tumor. These nonmalignant cells, rather than being "innocent bystanders", may actually be the active agents of metastatic disease.

The centers of solid tumors are frequently observed to be largely necrotic, resulting from prolonged hypoxia: insufficient availability of oxygen and glucose to meet the metabolic demands of the malignant cells. During tumor growth, the rapid proliferation of malignant cells places cells within the core of the tumor at increasingly larger distances from their nearest capillaries, drastically compromising blood flow to these cells. In addition to inducing necrosis, this isolation of cells with respect to the tumor vasculature renders the hypoxic areas of tumors inaccessible to virtually all molecular or nanoparticle-based therapies where delivery into the tumor is based on the EPR effect. This not only is a severe limitation to many standard therapeutic strategies such as chemotherapy[3] but also may limit the efficacy of many nanoparticle-based therapeutic approaches currently in development. In fact, one possible scenario for the progression of cancer to its latter, highly fatal stages is that cells which survive in these inaccessible hypoxic regions may themselves be the source of subsequent local recurrence and distant metastasis. It has been shown that hypoxia exerts a selective pressure on tumor cells in that only those with an aggressive phenotype (e.g., mutated p53) are able to survive in a low oxygen tension microenvironment.[4−6]

One of the body's responses to the presence of a malignant neoplasm is the recruitment of peripheral blood monocytes into the tumor, induced into the tumor mass by a chemoattractive gradient. Once the monocytes cross the endothelial basement membrane, they differentiate into macrophages.

* Corresponding author. Phone: (317) 278-3907. Fax (317) 278-3185. E-mail: sclare@iupui.edu.
[†] Department of Surgery, Indiana University School of Medicine.
[‡] Department of Chemistry, Rice University.
[§] Laboratory for Nanophotonics, Rice University.
[||] Birck Nanotechnology Center, Purdue University.
[⊥] Department of Pathology and Laboratory Medicine, Indiana University School of Medicine.
[#] Bindley BioScience Center, Purdue University.
[+] Department of Electrical and Computer Engineering, Rice University.

10.1021/nl072209h CCC: $37.00 
**Published on Web 11/03/2007**

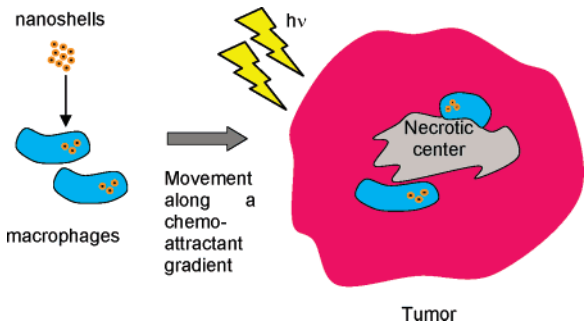


**Figure 1.** Schematic of Trojan Horse therapeutic nanoparticle delivery into the hypoxic region of tumor.

In breast cancer, macrophages may comprise up to 70% of the tumor mass.[7] Macrophages that have infiltrated a tumor are referred to as tumor-associated macrophages or TAMs. There is increasing evidence that suggests that TAMs are "educated" by their microenvironment and promote tumor progression.[8] The presence of large numbers of TAMs is associated with poor prognosis in breast cancer.[9,10] TAMs have been shown to foster invasion,[11−14] proliferation,[10,14−17] tumor neoangiogenesis,[8,18−20] and metastasis[12,14,20−25] and to suppress antitumor immune responses.[26−28]

Destruction of hypoxic regions within tumors, and especially the TAMs recruited into these regions, may well prevent the proliferation, growth, invasion, migration, and metastasis of malignant epithelial cells. This destruction should severely thwart tumor function and metastatic potential, directly impacting the probability of patient mortality. Delivery of therapeutics into the hypoxic regions of tumors, however, presents a major challenge. To address this problem, we hypothesize that the tumor's natural recruitment of monocytes may in fact be exploited for nanoparticle-based drug delivery and therapeutics. Since monocytes possess an innate phagocytotic capability and can be easily loaded with therapeutic nanoparticles, each cell can serve as a "Trojan Horse" delivery vector for nanoparticle therapeutics into these otherwise inaccessible tumor regions (Figure 1). In this treatment scenario, monocytes would be permitted to take up nanoparticle-based therapeutics and deliver them into the tumor site. Once recruited into the tumor, the monocytes differentiate into macrophages, which would also be required to maintain the cargo nanoparticles. The nanoparticle-laden macrophages would then migrate/chemotax to the hypoxic regions of the tumor. Once in place, the nanoparticle-based therapeutic function could be initiated by near-infrared (NIR) illumination into the tumor, destroying the TAMs. Depending on the illumination protocol, this therapeutic response may also include the destruction of adjacent cells or may be combined and coordinated with other chemical, molecular, or nanoparticle-based therapeutics, to result in total tumor destruction and remission with a greatly decreased risk of tumor regrowth and metastasis.

One essential requirement of this delivery and therapeutic strategy is that the intracellular cargo of the monocytes/macrophages remains inactive and harmless to its cellular host until delivery into the hypoxic tissue is accomplished. Au nanoshell-based photoinduced therapy is particularly amenable to this approach. Au nanoshells are nanoparticles consisting of a silica core surrounded by a thin Au shell.[29,30] By modifications of their relative core and shell dimensions, their plasmon resonances can be tuned such that they absorb light in the NIR,[31] a region of the spectrum where optical absorption of the tissue is minimal and penetration by the radiation is optimal for deep tissue treatments.[32] Au nanoshells can be designed and fabricated to either preferentially absorb or scatter light by varying the size of the particle relative to the wavelength of the light at their optical resonance.[32] Prior to resonant illumination, nanoshells are likely to remain entirely inert within cells or tissue, allowing for the viability of the monocytes/macrophages during recruitment into the tumor, differentiation to macrophages, and transport into hypoxic tumor regions. Upon illumination by NIR light at a wavelength corresponding to a nanoshell resonance, absorbed continuous wave (CW) laser light is converted to heat and has been shown to increase the temperature in the tissue in which the nanoshells are embedded by over 30 °C upon resonant illumination.[33] The resonant properties of nanoshells are dependent on their local environment,[34,35] and are preserved in the presence of defects or roughness on the nanoshell surface.[36,37] Nanoshell-based photothermal ablation therapy has been shown to successfully treat tumors in mice with tumor remission rates over 90%.[38]

Here we report the successful demonstration of several critical steps toward the ultimate goal of Trojan Horse therapeutics: the efficient phagocytosis of Au nanoshells by both monocytes and macrophages, photoinduced ablation of Au nanoshell-laden monocytes/macrophages, and the ability of nanoshell laden monocytes/macrophages to be taken up into a tumor and, once in place, to succumb to Au nanoshell-based photoinduced cell death using NIR light. Human breast tumor spheroids, an in vitro model of the hypoxic tumor microenvironment, were utilized to examine the efficacy of cellular uptake and nanoshell-assisted photoinduced ablation in the hypoxic tumor region using this approach.

Au nanoshells with a core radius 60 nm and shell thickness 27 nm were fabricated as previously described.[29] The internal and overall dimensions of the nanoparticles were confirmed using UV−visible extinction measurements, comparison with Mie scattering theory, and scanning electron microscopy (SEM). Absorbance spectra were obtained using a Varian Cary 5000 UV−vis-NIR spectrophotometer. SEM images were obtained using a FEI XL-30 environmental scanning electron microscope (ESEM). Figure 2 displays the extinction spectra of the Au nanoshells used, whose extinction peak maximum is at 754 nm. SEM images of these nanoshells are also shown.

Since monocytes become macrophages once they migrate from the capillary into the tumor, it is necessary to demonstrate Au nanoshell loading and subsequent survival in both monocytes and macrophages. To pursue this investigation, human whole blood was obtained from the Indiana Blood Center. Lymphocytes, monocytes, and platelets, i.e., the Buffy coat, were isolated using Ficoll density gradient centrifugation.[39] Monocytes were separated from the other components of the Buffy coat using anti-CD14 antibody

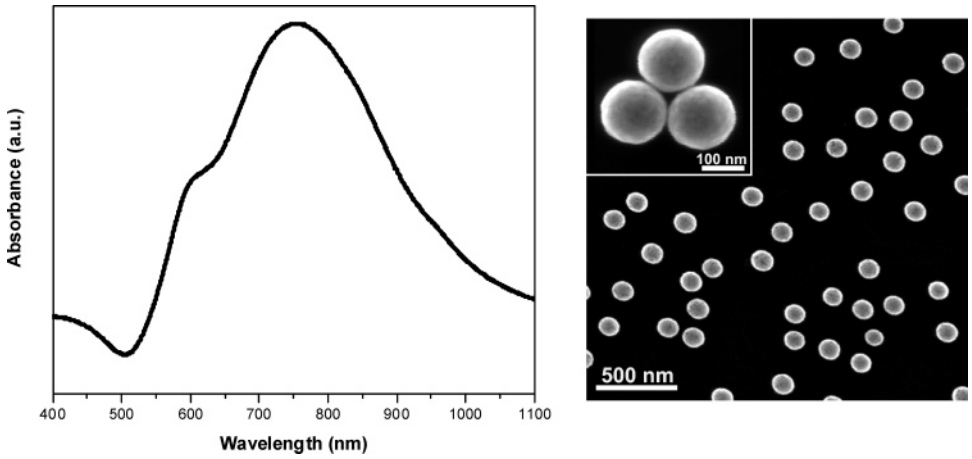


**Figure 2.** Left: Extinction spectra of $[r_1, r_2] = 60, 87$ nm Au nanoshells where $r_1$, $r_2$ denote the inner and outer Au shell layer radii, respectively. The peak extinction wavelength corresponds to the nanoshell surface plasmon resonance. Right: SEM images of the $[r_1, r_2] = 60, 87$ nm Au nanoshells at two different magnifications. The images reveal complete spherical shells (inset).

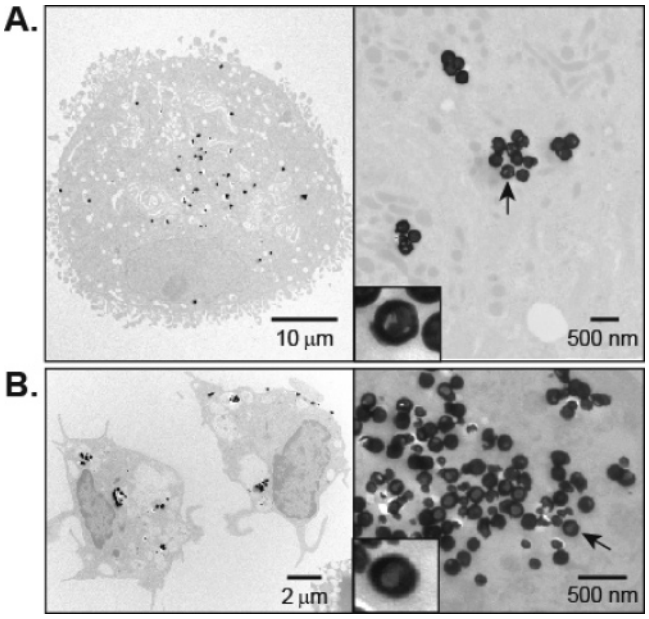


**Figure 3.** (A) Transmission electron micrograph of a nanoshell-laden macrophage. Au nanoshells are dispersed within vacuoles (left). Enlarged picture of aggregates of nanoshells in the macrophage in the right panel. The clear silica−core of the nanoshells surrounded with the black gold shells is shown in the inset (arrow). (B) Transmission electron micrograph of a nanoshell-laden monocytes.

bound to magnetic beads (MACS cell separation system, Miltenyi Biotec, Auburn, CA). Monocytes were differentiated into macrophages in vitro by culturing the isolated monocytes for 7 days in Teflon bags in the presence of recombinant human macrophage-colony stimulating factor (R & D Systems, Minneapolis, MN).[40] Macrophages or monocytes were incubated with Au nanoshells for 24 h. Figure 3 shows a transmission electron microscope (TEM) images of phagocytosed Au nanoshells in macrophages and monocytes. When the Au nanoshells are phagocytosed, they are taken up in vacuoles and dispersed in the cytoplasm. Uptake of Au nanoshells into monocytes and macrophages was observed to be equally effective. It can be observed in these images that the intracellular environment may modify and somewhat reshape the morphology of the nanoparticle's shell layer. This reshaping has been observed in the context of several types of chemical treatments,[41,42] and can be minimized by suitable functionalization of the nanoparticles prior to use. It is important to note, however, that the defects observed in the nanoshells in these images would not be sufficient to destroy their resonant optical absorption properties.[36,37]

To determine the treatment parameters for producing optimal macrophage destruction in vitro, macrophages loaded with Au nanoshells and control macrophages (without nanoshells) were irradiated using varying power densities and irradiation durations. Twenty thousand macrophages in 200 $\mu$L of Macrophage-SFM (serum free medium) (Gibco, Invitrogen, Carlsbad, CA) per well in a 96-well plate were incubated with unfunctionalized Au nanoshells overnight. An identical number of macrophages were used as a control sample. One microliter of propidium iodide (PI, 1 mg/mL in phosphate-buffered saline), normally cell impermeant at this concentration, was added to each well of the microtiter plate to study the membrane damage caused by photoinduced ablation of the macrophages. Macrophage death was quantified using the Cytotoxicity Detection Kit (Roche Applied Science, Indianapolis, IN). This assay is a colorimetric assay which measures the amount of lactate dehydrogenase (LDH) released from the cytosol of damaged cells into the supernatant. The NIR irradiation source as well as the visualization system used in our study was a Bio-Rad Radiance 2100 MP Rainbow Confocal/Multiphoton System. The laser source produces pulses with widths of 100 fs at a repetition rate of 80 MHz, and in our experiments this pulsed laser excitation was used to investigate protocols and characteristics of Au-nanoshell-based photoinduced cell death in this very different ablation regime. The total power at the source was 1.54 W at 754 nm. The cells were scanned through a 4× microscope objective within a fixed 1028 $\mu$m × 1028 $\mu$m area. A single scan was performed in 1 s at 500 lines/s, in which the 1028 $\mu$m × 1028 $\mu$m area is divided into the 500 lines. The pixel dwell time was on the order of 2.6 $\mu$s over a pixel area of approximately 2 $\mu$m × 2 $\mu$m. Immediately after

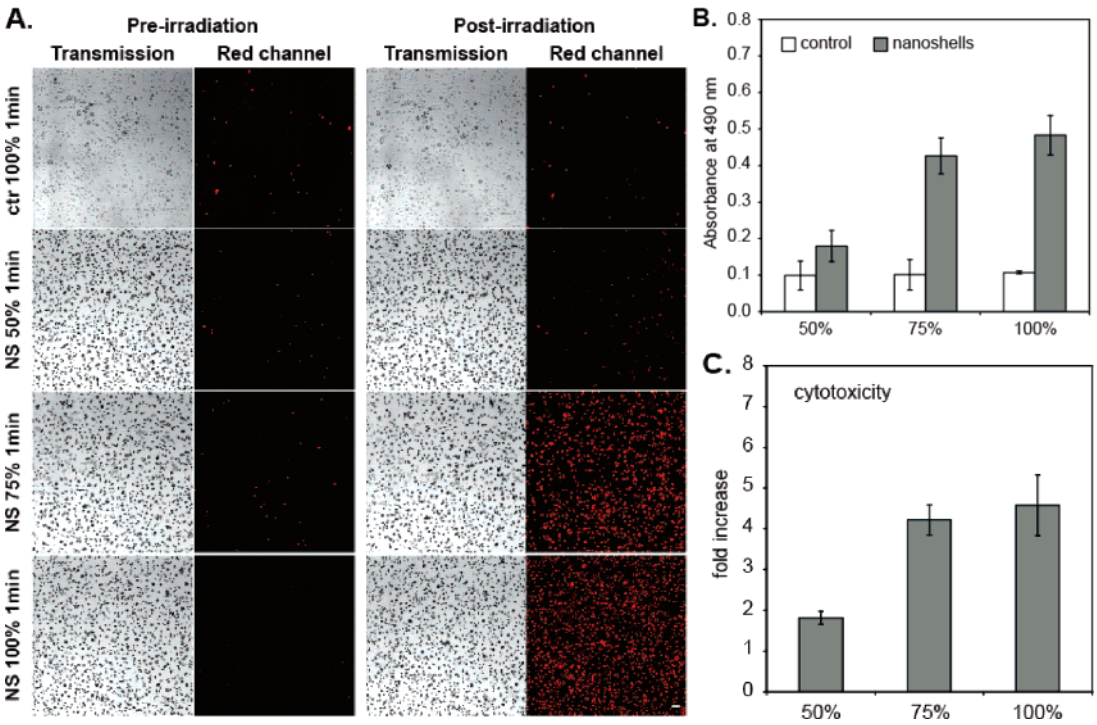


**Figure 4.** Effect of increasing power on the cytotoxicity of macrophages. Power was increased from 50% to 100% in increments of 25%. (A) Increasing PI uptake with increasing laser power: ctr, macrophages alone; NS, macrophages loaded with gold−silica nanoshells. Scale bar is 50 $\mu$m in A (bottom, right corner). (B and C) Determination of cytotoxicity after irradiation. Supernatant was removed from the irradiated wells, and the activity of the released LDH was measured.

irradiation, a transmission image and red channel image were acquired using the 10× objective of the confocal microscope, and the images were overlaid. Power at the source was varied in increments of 25%. All experiments were repeated in triplicate.

Upon the irradiation of the nanoshell-laden cells, a dose−response corresponding to increasing uptake of propidium iodide (Figure 4A) and release of LDH (Figure 4B,C) as a function of power is observed. Irradiation with 75% laser power showed a cytotoxic effect comparable to 100% laser power. Control macrophages without Au nanoshells showed no PI uptake as well as no increase in the release of LDH. A 75% laser power produced effective photothermal ablation of TAMs, and therefore, this power density was utilized in the subsequent duration experiments.

The macrophages were then irradiated at 75% power to determine the optimum duration of NIR irradiation for cell destruction. By visual inspection, the amount of PI uptake appears relatively similar at all time points (Figure 5). However, quantification of the PI signal (Supporting Information) reveals that PI uptake is greatest at 10 s of irradiation. This is confirmed by the observed LDH release: the extent of cytotoxicity is greatest at 10 s irradiation duration. However, given the error of the measurements, the cytotoxicities at 10 and 30 s are not significantly different. The cytotoxicity assay for the sample irradiated at 75% for 1 min showed almost the same increase (4×) of LDH release (Figure 4C). These results are as expected since, in the two-photon system used, the time of irradiation (*x*-axis in parts B and C of Figure 5) indicates the number of scans, where each scan is performed in 1 s. Thus for the 10 s case, 10 consecutive scans are performed and the time between irradiation of each 2.6 $\mu$m × 2.6 $\mu$m pixel would still be about 1 s. Performing additional scans at 1 Hz did not cause additional cell damage, indicating that at this scan rate, accumulated thermal effects are negligible and the photoinduced ablation resulting from the initial 10 scans is sufficient to cause lethal cell damage. It should also be noted that at any given time a region smaller than an individual cell is being illuminated (2.6 $\mu$m × 2.6 $\mu$m) and, hence, the mechanism of cell death may also include localized disruption of the cell membrane or local thermal ablation of vital intracellular compartments. Further experiments are warranted to examine the differences between femtosecond and CW Au-nanoshell-based photoinduced cell death in greater physiological detail and present an opportunity to understand the mechanism of cell death based on disruption of intracellular components, e.g., organelles.

The hypoxic tumor microenvironment can be modeled in vitro using tumor spheroids. These structures, composed of malignant breast epithelial cells, have a central necrotic area of cell debris surrounded by layers of hypoxic cells; the outer layer is comprised of normoxic cells (Supporting Information). Lewis and colleagues[43] have shown that macrophages infiltrate the spheroid and accumulate in the inner hypoxic rim around the central necrosis. Breast tumor spheroids were established by culturing human T47D cells on agarose for 20 days at 37 °C, 5% $CO_2$. The culture medium was replaced with fresh culture medium on alternate days. Five thousand macrophages and 8.3 × $10^8$ gold−silica nanoshells were added to each well of a 96-well plate; each well contained a single spheroid. The spheroids, macrophages, and nanoshells

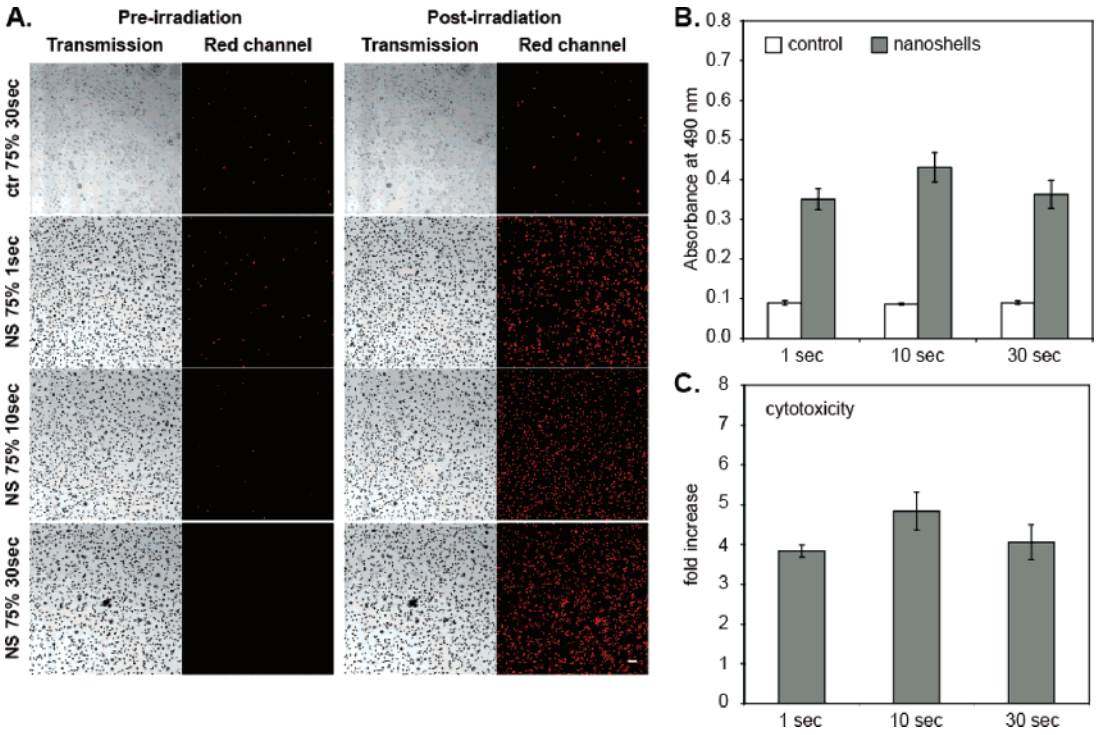


**Figure 5.** Effect of increasing irradiation duration on the cytotoxicity of macrophages. Macrophages loaded with gold−silica nanoshells were irradiated at 754 nm at 75% power for 1, 10, and 30 s, respectively. (A) PI uptake does not appear markedly different at the three time points. Scale bar is 50 $\mu$m in A (bottom, right corner). (B and C) The amount of LDH released increases between 1 and 10 s. Additional irradiation does not result in an increase in cytotoxicity (30 s). All experiments were repeated in triplicate.

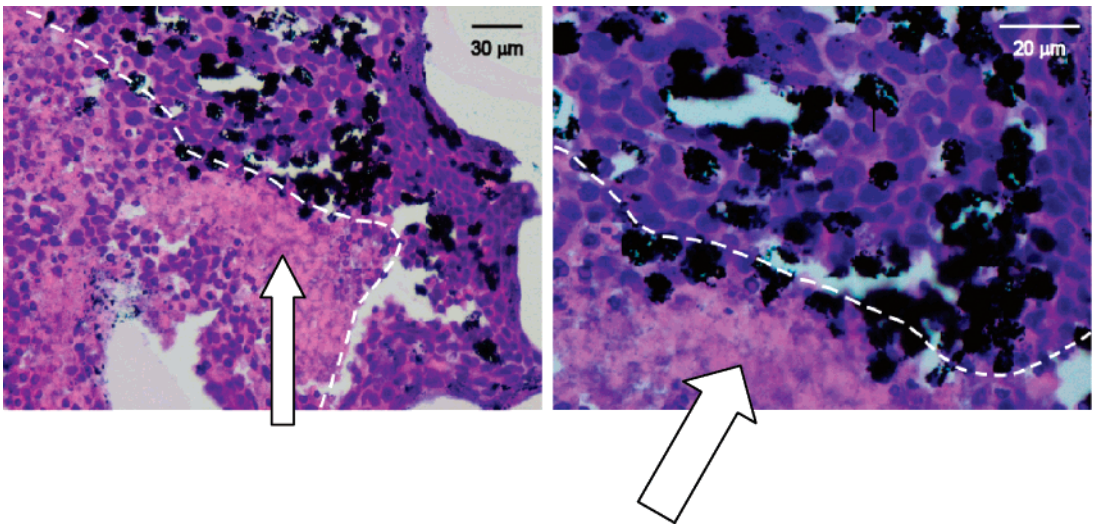


**Figure 6.** Photomicrograph of hematoxylin and eosin stained section of T47D tumor spheroid infiltrated with nanoshell-laden macrophages: left, 40×; right, 100×. Scale included in photomicrographs. The nanoshell-laden macrophages (black areas) have infiltrated the spheroid and reside within the viable tumor cells as well as near areas of necrosis (pink staining; white arrow). The dotted red line divides the central area of necrosis (white arrow) from the rim of viable cells which stain a dark purple due to the presence of nuclei.

were incubated for 3 days at 37 °C, 5% $CO_2$. Phagocytosis of the Au nanoshells as well as infiltration of macrophages into the tumor spheroid was monitored by transmission light microscopy and confirmed by H & E staining. The infiltrated macrophages accumulate within the hypoxic rim and around the central necrosis (Figure 6). The tumor spheroids had reached approximately 780 $\mu$m in diameter at the time of irradiation. The T47D breast tumor spheroids infiltrated with macrophages were irradiated through the 10× microscope objective of the Bio-Rad Radiance 2100 MP Rainbow Confocal/Multiphoton System at 100% power for 2 s (i.e., Two scans). Tumor spheroid infiltrated with macrophages without nanoshells were utilized as a control. A green fluorescent dye (CellTracker, Molecular Probes, Invitrogen, Carlsbad, CA) was added to each well plate to facilitate identification of cells. After irradiation, a transmission image and a green as well as a red channel image were acquired using the 10× objective of the confocal microscope, and the images were overlaid (Figure 7). Irradiation of a tumor spheroid infiltrated with nanoshell-laden macrophages re-

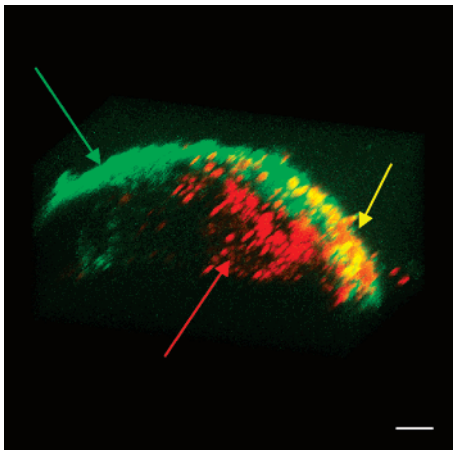

**Figure 7.** Frame from three-dimensional reconstruction of tumor spheroid. Perspective: looking out from necrotic center toward normoxic rim of cells. Viable cells (green fluorescence) form an outer shell around the central necrosis: green arrow, unirradiated T47D cells; red arrow, nanoshell-laden macrophages which have infiltrated into the area cell debris and necrosis in the center of the spheroid. Macrophages are propidium iodide positive following irradiation. Yellow cells/arrow: May represent T47D cells which have been thermally damaged due to their location next to macrophages. Cells to the left in the photo (green arrow) have not been irradiated, serving as an internal control. Scale bar is 50 $\mu$m.

sulted in death of cells within the irradiated area which are identified by propidium iodide fluorescence (Figure 7). There are no viable malignant epithelial cells in the center of the spheroid; this area is composed of cellular debris/necrotic cells. The area of red signal toward the center of the spheroid is from thermally damaged macrophages which were attracted into the center by signals released by the cellular debris.[44] Macrophages are also recruited to areas of hypoxia within the rim of viable malignant epithelial cells by a chemoattractant gradient established by the anoxic and hypoxic cells. This results in the intercalation of the macrophages among the epithelial cells as seen in Figure 6 and Supporting Information. Yellow-orange fluorescence in the outer layer of the spheroid as seen in Figure 7 may represent damaged/dead T47D tumor cells. The irradiation of the control spheroid with nonladen macrophages under the same conditions showed no increase in the number of dead cells. The extent to which femtosecond laser versus CW laser ablation may be more effective at destroying the extended hypoxic region based Trojan Horse delivery is the subject of future experiments.

In conclusion, we have reported the successful demonstration of several critical steps toward the ultimate goal of Trojan Horse nanoparticle delivery and therapeutics. The efficient phagocytosis of Au nanoshells by both monocytes and macrophages, photoinduced ablation of Au-nanoshell-laden monocytes/macrophages, tumor recruitment, and photoinduced cell death of macrophages in the hypoxic microenvironment of a human breast tumor spheroid have all been successfully demonstrated. It was observed that even though the irradiation source focuses the energy within subcellular volumes, cell death resulted for incident laser powers above a power threshold. This may indicate that nanoshell-based photoinduced ablation using femtosecond NIR sources may be a consequence of local subcellular thermal ablation. Although the essential steps for Trojan Horse delivery have been demonstrated specifically for nanoshell-based therapy, this general approach might be useful for delivery of a large variety of therapies to the hypoxic regions in tumors. Such therapies may be either nanoparticle or molecule based, developed with the requirement that the cell's cargo remains noncytotoxic until the macrophages enter the tumors' hypoxic regions. Infrared-stimulated photothermal therapeutics using Au nanorods or carbon nanotubes, nanoparticle-based therapeutics triggered by application of external magnetic fields, or molecular therapies activated by the unique chemical microenvironment of the hypoxic region may all be ultimately suitable for this delivery mechanism.

**Acknowledgment.** This work is supported by a pilot grant awarded by the Indiana University/Purdue University Cancer Centers/Oncological Sciences Center Collaborative Grants Program, the U.S. Army Medical Research and Materiel Command, 820 Chandler Street, Fort Detrick, MD 21702-5014, under Grant No. DAMD17-03-1-0384 issued to Rice University, National Aeronautics and Space Administration Grant 68371, Robert A. Welch Foundation Grant C-1220, a training fellowship from the Keck Center Nanobiology Training Program of the Gulf Coast Consortia, and NIH Grant No. 1 T90 DK070121−01.

**Supporting Information Available:** Description of analysis of cell membrane damage as a function of irradiation duration. Photomicrographs of hematoxylin and eosin stained sections of tumor spheroids at varying magnification. This material is available free of charge via the Internet at http://pubs.acs.org.

## References

(1) Maeda, H.; Wu, J.; Sawa, T.; Matsumura, Y.; Hori, K. *J. Controlled Release* **2000**, *65*, 271−284.
(2) Loo, C.; Lowery, A.; Halas, N.; West, J.; Drezek, R. *Nano Lett.* **2005**, *5*, 709−711.
(3) Primeau, A. J.; Rendon, A.; Hedley, D.; Lilge, L.; Tannock, I. F. *Clin. Cancer Res.* **2005**, *11*, 8782−8788.
(4) Brown, J. M. *Cancer Res.* **1999**, *59*, 5863−5870.
(5) Cairns, R. A.; Khokha, R.; Hill, R. P. *Curr. Mol. Med.* **2003**, *3*, 659−671.
(6) Christofori, G. *Nature* **2006**, *441*, 444−450.
(7) Kelly, P. M.; Davison, R. S.; Bliss, E.; McGee, J. O. *Br. J. Cancer* **1988**, *57*, 174−177.
(8) Lewis, C. E.; Pollard, J. W. *Cancer Res.* **2006**, *66*, 605−612.
(9) Leek, R. D.; Landers, R. J.; Harris, A. L.; Lewis, C. E. *Br. J. Cancer* **1999**, *79*, 991−995.
(10) Tsutsui, S.; Yasuda, K.; Suzuki, K.; Tahara, K.; Higashi, H.; Era, S. *Oncol. Rep.* **2005**, *14*, 425−431.
(11) Lin, E. Y.; Nguyen, A. V.; Russell, R. G.; Pollard, J. W. *J. Exp. Med.* **2001**, *193*, 727−740.
(12) Hagemann, T.; Robinson, S. C.; Schulz, M.; Trümper, L.; Balkwill, F. R.; Binder, C. *Carcinogenesis* **2004**, *25*, 1543−1549.
(13) Hagemann, T.; Wilson, J.; Kulbe, H.; Li, N. F.; Leinster, D. A.; Charles, K.; Klemm, F.; Pukrop, T.; Binder, C.; Balkwill, F. R. *J. Immunol.* **2005**, *175*, 1197−1205.
(14) Goswami, S.; Sahai, E.; Wyckoff, J. B.; Cammer, M.; Cox, D.; Pixley, F. J.; Stanley, E. R.; Segall, J. E.; Condeelis, J. S. *Cancer Res.* **2005**, *65*, 5278−5283.
(15) O'Sullivan, C.; Lewis, C. E.; Harris, A. L.; McGee, J. O. *Lancet* **1993**, *342*, 148−149.
(16) Lewis, C.; Murdoch, C. *Am. J. Pathol.* **2005**, *167*, 627−635.

(17) van Netten, J. P.; George, E. J.; Ashmead, B. J.; Fletcher, C.; Thornton, I. G.; Coy, P. *Lancet* **1993**, *342*, 872−873.
(18) Sunderkotter, C.; Goebeler, M.; Schulze-Osthoff, K.; Bhardwaj, R.; Sorg, C. *Pharmacol. Ther.* **1991**, *51*, 195−216.
(19) Lewis, C. E.; Leek, R.; Harris, A.; McGee, J. O. *J. Leukocyte Biol.* **1995**, *57*, 747−751.
(20) Leek, R. D.; Lewis, C. E.; Whitehouse, R.; Greenall, M.; Clarke, J.; Harris, A. L. *Cancer Res.* **1996**, *56*, 4625−4629.
(21) Mantovani, A.; Sozzani, S.; Locati, M.; Allavena, P.; Sica, A. *Trends Immunol.* **2002**, *23*, 549−555.
(22) Hanada, T.; Nakagawa, M.; Emoto, A.; Nomura, T.; Nasu, N.; Nomura, Y. *Int. J. Urol.* **2000**, *7*, 263−269.
(23) Wyckoff, J.; Wang, W.; Lin, E. Y.; Wang, Y.; Pixley, F.; Stanley, E. R.; Graf, T.; Pollard, J. W.; Segall, J.; Condeelis, J. *Cancer Res.* **2004**, *64*, 7022−7029.
(24) Ohno, S.; Ohno, Y.; Suzuki, N.; Kamei, T.; Koike, K.; Inagawa, H.; Kohchi, C.; Soma, G.; Inoue, M. *Anticancer Res.* **2004**, *24*, 3335−3342.
(25) Oosterling, S. J.; van der Bij, G. J.; Meijer, G. A.; Tuk, C. W.; van Garderen, E.; van Rooijen, N.; Meijer, S.; van der Sijp, J. R.; Beelen, R. H.; van Egmond, M. *J. Pathol.* **2005**, *207*, 147−155.
(26) Zeineddine, N. S.; Avina, M. D.; Williams, C. C.; Wepsic, H. T.; Jadus, M. R. *Immunol. Lett.* **1999**, *70*, 63−68.
(27) Elgert, K. D.; Alleva, D. G.; Mullins, D. W. *J. Leukocyte Biol.* **1998**, *64*, 275−290.
(28) Wojtowicz-Praga, S. *J. Immunother.* **1997**, *20*, 165−177.
(29) Oldenburg, S. J.; Averitt, R. D.; Westcott, S. L.; Halas, N. *Chem. Phys. Lett.* **1998**, *288*, 243−247.
(30) Prodan, E.; Radloff, C.; Halas, N. J.; Nordlander, P. *Science* **2003**, *302*, 419−422.
(31) Prodan, E.; Nordlander, P. *Nano Lett.* **2003**, *3*, 543−547.
(32) Loo, C.; Lin, A.; Hirsch, L.; Lee, M. H.; Barton, J.; Halas, N.; West, J.; Drezek, R. *Technol. Cancer Res. Treat.* **2004**, *3*, 33−40.
(33) Hirsch, L. R.; Stafford, R. J.; Bankson, J. A.; Sershen, S. R.; Rivera, B.; Price, R. E.; Hazle, J. D.; Halas, N. J.; West, J. L. *Proc. Natl. Acad. Sci. U.S.A.* **2003**, *100*, 13549−13554.
(34) Prodan, E.; Lee, A.; Nordlander, P. *Chem. Phys. Lett.* **2002**, *360*, 325−332.
(35) Tam, F.; Moran, C.; Halas, N. *J. Phys. Chem. B* **2004**, *198*, 17290−17294.
(36) Oubre, C.; Nordlander, P. *J. Phys. Chem. B* **2004**, *108*, 17740−17747.
(37) Wang, H.; Fu, K.; Drezek, R.; Halas, N. *J. Appl. Phys. B* **2006**, *84*, 191−196.
(38) O'Neal, D. P.; Hirsch, L. R.; Halas, N. J.; Payne, J. D.; West, J. L. *Cancer Lett.* **2004**, *209*, 171−176.
(39) http://www6.amershambiosciences.com/applic/upp00738.nsf/vLookupDoc/224505666−P516/$file/71716700AF.pdf.
(40) van der Meer, J. W.; van de Gevel, J. S.; Blussé van Oud Alblas, A.; Kramps, J. A.; van Zwet, T. L.; Leijh, P. C.; van Furth, R. *Immunology* **1982**, *47*, 617−625.
(41) Aguirre, C. M.; Kaspar, T. R.; Radloff, C.; Halas, N. J. *Nano Lett.* **2003**, *3*, 1707−1711.
(42) Wang, H.; Goodrich, G. P.; Tam, F.; Oubre, C.; Nordlander, P.; Halas, N. *J. Phys. Chem. B* **2005**, *109*, 11083−11087.
(43) Owen, M. R.; Byrne, H. M.; Lewis, C. E. *J. Theor. Biol.* **2004**, *226*, 377−391.
(44) Azenshtein, E.; Luboshits, G.; Shina, S.; Neumark, E.; Shahbazian, D.; Weil, M.; Wigler, N.; Keydar, I.; Ben-Baruch, A. *Cancer Res.* **2002**, *62*, 1093−1102.
(45) http://rsb.info.nih.gov/ij/.

NL072209H